Compact, low power radio frequency cavity for femtosecond electron microscopy

AIP | Review of Scientific Instruments

Compact, low power radio frequency cavity for femtosecond electron microscopy

A. Lassise, P. H. A. Mutsaers, and O. J. Luiten

Citation: Rev. Sci. Instrum. **83**, 043705 (2012); doi: 10.1063/1.3703314
View online: http://dx.doi.org/10.1063/1.3703314
View Table of Contents: http://rsi.aip.org/resource/1/RSINAK/v83/i4
Published by the American Institute of Physics.

Related Articles

Fine-tuning of whispering gallery modes in on-chip silica microdisk resonators within a full spectral range
Appl. Phys. Lett. 102, 041104 (2013)

Chiroptical hot spots in twisted nanowire plasmonic oscillators
Appl. Phys. Lett. 102, 043103 (2013)

The plasmonic J-pole antenna
Appl. Phys. Lett. 102, 033106 (2013)

Electro-optic sensor for specific absorption rate measurements
Appl. Phys. Lett. 102, 033502 (2013)

Cavity piezooptomechanics: Piezoelectrically excited, optically transduced optomechanical resonators
Appl. Phys. Lett. 102, 021110 (2013)

Additional information on Rev. Sci. Instrum.

Journal Homepage: http://rsi.aip.org
Journal Information: http://rsi.aip.org/about/about_the_journal
Top downloads: http://rsi.aip.org/features/most_downloaded
Information for Authors: http://rsi.aip.org/authors

ADVERTISEMENT

Compact, low power radio frequency cavity for femtosecond electron microscopy

A. Lassise, P. H. A. Mutsaers, and O. J. Luiten[a)]
Department of Applied Physics, Eindhoven University of Technology, P.O. Box 513, 5600 MB Eindhoven, The Netherlands

(Received 21 October 2011; accepted 26 March 2012; published online 17 April 2012)

Reported here is the design, construction, and characterization of a small, power efficient, tunable dielectric filled cavity for the creation of femtosecond electron bunches in an existing electron microscope without the mandatory use of femtosecond lasers. A 3 GHz pillbox cavity operating in the TM_{110} mode was specially designed for chopping the beam of a 30 keV scanning electron microscope. The dielectric material used is $ZrTiO_4$, chosen for the high relative permittivity ($\varepsilon_r = 37$ at 10 GHz) and low loss tangent ($\tan\delta = 2 \times 10^{-4}$). This allows the cavity radius to be reduced by a factor of six, while the power consumption is reduced by an order of magnitude compared to a vacuum pillbox cavity. These features make this cavity ideal as a module for existing electron microscopes, and an alternative to femtosecond laser systems integrated with electron microscopes. [http://dx.doi.org/10.1063/1.3703314]

I. INTRODUCTION

A. Motivation

A time-resolved technique for electron microscopes has been desired since the first glimpse into the minuscule world, early interest beginning with electron stroboscopic microscopy in the 1970s resolving motion down to nanoseconds (Plows and Nixon[1]) and eventually picoseconds (Oldfield,[2] Gopinath and Hill,[3] Hieke and Meusburger,[4] Sadorf and Kratz[5]), with a resolution dropping down to 0.2 ps (Ura *et al.*[6]).

Radio frequency (RF) cavities were suggested, developed, and investigated thoroughly in the 1970s by Oldfield[7] and Ura *et al.*[6] The motivation of Oldfield was to use the cavities as time-dependent lenses in order to circumvent Scherzer's theorem in an attempt to defeat spherical aberration (Hawkes and Casper[8]). They demonstrated that aberration correction could be done with time-dependent cavities, but required short pulses that would only sample a particular phase of the field within the cavity. These systems proved to be cumbersome and less versatile than yearned for in the microscopy community.

Recent interest again has been piqued as technology has allowed femtosecond laser systems to be incorporated with electron microscopes: the advent of ultrafast electron microscopy (UEM), ultrafast electron diffraction (UED), and ultrafast electron crystallography (UEC) (Gahlmann *et al.*,[9] Shorokhov and Zewail,[10] Zewail[11]). Femtosecond resolved electron energy loss spectroscopy (FEELS) has been carried out at a repetition rate of 100 kHz and 1 MHz, with less than one electron per bunch (Carbone *et al.*[12]). In recent advances a laser focused on a photocathode (Yang *et al.*,[13] van Oudheusden *et al.*,[14] Cao *et al.*[15]) or upon the tip of an existing electron microscope (Armstrong *et al.*,[16] Park *et al.*,[17] Yurtsever and Zewail[18]) have all successfully produced femtosecond electron bunches. Simulations and theory have predicted femtosecond electron bunch creation through interaction between an electron bunch and the ponderomotive potential of a femtosecond laser pulse (Baum and Zewail[19]). Photoelectron emission microscopy (PEEM) has demonstrated methods of time-resolved measurements with the accuracy resolved down into the attosecond regime (Kubo *et al.*[20]). In all of these examples, electron bunches were created with a femtosecond resolution, breaking the earlier barrier, but all requiring femtosecond laser systems to be incorporated.

The work of Oldfield[2,7] and Ura *et al.*[6] with RF cavities has once again been revived due to technological advances in RF technology, allowing higher quality equipment to be developed at lower costs. Along with the RF advancements, synchronization with femtosecond laser systems has been achieved (Kiewiet *et al.*[21]), allowing for compression of picosecond bunches into the femtosecond regime (van Oudheusden).

In this paper the design, construction, and commissioning of an RF device is presented which enables generation of ~100 fs electron pulses at a repetition rate much greater than 1 MHz. The device is inexpensive and compact enough to be incorporated in an existing electron microscope, constituting an affordable alternative for laser-based UEM, UED, UEC, and FEELS systems employed in research.

To realize ~100 fs electron bunches at a rep. rate $\gg$ 1 MHz, a resonant RF cavity is used to sweep an electron microscope's dc beam across a slit. The cavity-slit combination employed on a continuous beam can create the short bunches if the transverse sweep is large compared to the size of the slit. This can be achieved with a small slit in combination with either a large field amplitude in the cavity, or a long distance from cavity to slit. The repetition rate of the bunches will then be twice the period of the cavity's resonant frequency, and the length of the bunches much less than half a period of the resonant oscillation. For a cavity with a resonance at 3 GHz, the period is 333 ps. For 1 μA

a)Electronic mail: O.J.Luiten@tue.nl.

chopped to 100 fs bunches, the charge per bunch will be about one electron per bunch, similar to FEELS experiments.

This method has several practical advantages compared to systems using femtosecond lasers. The first is that in principle, arbitrarily short pulses are possible, only limited by slit width s, the distance between cavity and slit l, and the RF field amplitude. The second is a higher beam quality, i.e., transverse emittance and brightness, as both simulations and measurements have suggested that beam quality is relatively unperturbed, preserving the transverse emittance within the bunch. The third is a higher average current due to the higher repetition rate. This leads to shorter sampling times for experiments.

Synchronization of the cavity with a femtosecond laser system can be achieved with an accuracy of less than 20 fs (Kiewiet *et al.*[21]). This would further extend the abilities to perform pump-probe experiments for the electron microscopy community. The typical maximum fluence for a pump-probe experiment is approximately 1 nJ/μm^2. A standard Ti:Sapphire oscillator for a femtosecond laser system typically emits 5–10 nJ/pulse. If the laser is focused to a 10 μm^2 spot, the fluence from just the Ti:Sapphire oscillator is sufficient for pump-probe experiments. Further more, Ti:S lasers have been built with repetition rates well into the GHz regime (Fortier *et al.*,[22] Bartels *et al.*[23,24]). Synchronized with the proposed cavity at 3 GHz would give pump-probe capabilities with an average current of $\sim$1 nA.

To be implemented as a module into existing electron microscopes, the cavity should preferably be compact and have low power consumption. Low power consumption is to minimize the heat load on a microscope, as well as the cost of RF amplifiers. To realize the compact size and low power consumption, a dielectric with a high relative permittivity ε_r, and a low loss tangent tan δ will be employed.

A dielectric material is chosen because for a given resonant frequency, the wavelength of the RF field decreases, in comparison to a vacuum pillbox cavity, by a factor of $\varepsilon_r{}^{-1/2}$, leading to a decrease in size of the cavity by $\varepsilon_r{}^{-1/2}$. In addition, the electric field also is decreased by $\varepsilon_r{}^{-1/2}$, which combined with the reduced size leads to a decrease in the overall power consumption of the cavity by $\varepsilon_r{}^{-1}$. The insertion of a dielectric material leaves the oscillating magnetic field strength unaffected and thus implies the use of a magnetic field for the interaction. To realize an oscillating magnetic field of sufficient strength, a resonant RF cavity is employed.

B. Organization

The remaining paper is structured in five sections. In Sec. II, first the general principle of the method will be discussed, yielding an estimate for the required magnetic field amplitude. Next, using the electromagnetic field distribution in a resonant, idealized pillbox cavity, the power consumption, quality factor, and cavity size are calculated for a copper pillbox resonating at 3 GHz in the TM_{110} mode, filled either with vacuum or $ZrTiO_4$ (a ceramic chosen for high dielectric constant and relatively low loss). These analytical calculations form the basis for the design. In practice, the cavity geometry deviates from the perfect pillbox. In Sec. III, numerical simulations are used to calculate the EM field distribution, power loss, and quality factor for the realistic cavity, and then compared to the analytical idealized pillbox of Sec. II. In Sec. IV, the dielectric filled TM_{110} cavity that has been constructed is characterized by measuring resonant frequency, quality factor, the on-axis field profile, and the tunability of the resonant frequency. Sec. V consists of the implementation and discussion of the cavity in the scanning electron microscope (SEM) beamline. Fast streaking of the SEM dc beam is demonstrated. By placing a slit into the streaked beam, ultra-short pulses are produced. To establish whether the electron beam quality is affected by RF chopping, the emittances of both the dc beam entering the cavity and the chopped beam are measured by means of a quadrupole waist scan. An increase in emittance due to chopping is observed, in agreement with numerical charged particle tracking simulations. Finally, in Sec. VI the results are summarized and discussed.

II. THEORY

In this section, the general principle of RF chopping will be discussed. The fields and power loss in a dielectric filled pillbox cavity operating in the TM_{110} mode are treated analytically.

A. Principle of RF chopping

An electron is moving along the z axis with velocity $\vec{v} = v_e\hat{z}$. A slit of size s is placed at a distance l from the cavity, along the electron trajectory, as seen in Figure 1. With the cavity centered around $z = 0$, the slit extends over the range $\frac{-s}{2} \leq x \leq \frac{s}{2}$ at $z = l + d/2$. Assume a uniform magnetic field $\vec{B}$ along the electron trajectory inside the cavity oscillating with amplitude B_0 and radial frequency $\omega = 2\pi f_0$,

$$\vec{B} = B_o \cos(\omega t + \varphi_o)\hat{y}, \tag{1}$$

with t the time the electron enters the cavity and φ_0 the phase at $t = 0$. Since the transverse velocity kick imparted by the cavity will be much smaller than v_e, we approximate the velocity over the entire trajectory by $\vec{v} \approx v_e\hat{z}$. The Lorentz force $\vec{F} = q\vec{v} \times \vec{B}$ acting on the electron will thus lead to a momentum kick in the x-direction,

$$\vec{p} = \frac{qv_eB_0}{\omega}\left[\sin(\omega t_1 + \varphi_0) - \sin(\varphi_0)\right]\hat{x}, \tag{2}$$

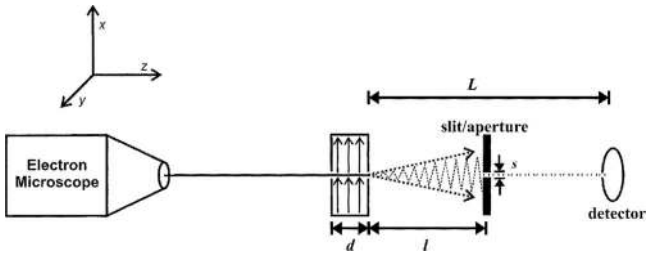

FIG. 1. A general schematic of how an RF cavity and slit are used in tandem with an electron microscope to create a regular train of electron bunches.

with $t_1 = d/v_e$ being the cavity transit time. The maximum deflection

$$p_{x,\max} = -\frac{2qv_eB_0}{\omega}\sin(\varphi_0), \tag{3}$$

occurs for $t_1 = \pi/\omega$, corresponding to a transit time equal to half of a period of the cavity, i.e., a cavity length given by $d = \pi v_e/\omega$. The corresponding sweep angle α of the electron trajectory with the z axis is given by

$$\alpha(\varphi_0) = \frac{p_{x,\max}}{mv_e} = -\frac{2qB_0}{m\omega}\sin(\varphi_0), \tag{4}$$

where the small angle approximation was used. Only those electrons will get through the slit whose entrance phase is such that the sweep angle is smaller than the angle subtended by the slit, i.e., $|\alpha(\varphi_0)| < s/2l$. Since the slit is centered on the z axis and, by assumption, $|\varphi_0| \ll 1$, it follows that only those electrons will get through the slit whose entrance phase φ_0 lies in the range

$$-\frac{sm\omega}{4lqB_0} < \varphi_0 < \frac{sm\omega}{4lqB_0}, \tag{5}$$

corresponding to a bunch length

$$\Delta t_{bunch} \equiv \frac{\Delta\varphi_0}{\omega} = \frac{sm}{2lqB_o}. \tag{6}$$

To achieve a bunch length of ~100 fs, modest values of $s = 10\ \mu$m, $l = 10$ cm, and $B_0 = 3$ mT are needed. To realize an oscillating magnetic field of 3 mT with minimal power consumption, a resonant RF cavity is used.

B. Dielectric filled pillbox cavity

We start from a standard cylindrical dielectric material surrounded by perfectly conducting metallic walls with radius a in the xy-plane, and length d in the z-direction, as seen in Figure 2. The criterion of a magnetic field transverse to the direction of electron propagation, z, implies the use of a transverse magnetic (TM) mode. The lowest TM mode, TM_{010} or monopole mode, is characterized by a longitudinal electric field $\vec{E} = E\hat{z}$, which is maximal at $r = 0$, and an azimuthal magnetic field $\vec{B} = B\hat{\varphi}$, which is zero at $r = 0$. The TM_{010} mode is used for particle acceleration and longitudinal bunch compression (van Oudheusden,[10] Chao and Tigner[25]). The next mode higher in frequency, TM_{110} or dipole mode, also has a longitudinal electric field, which is,

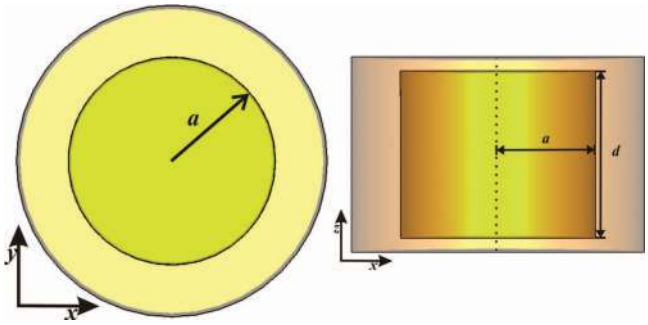

FIG. 2. An ideal dielectric filled pillbox cavity.

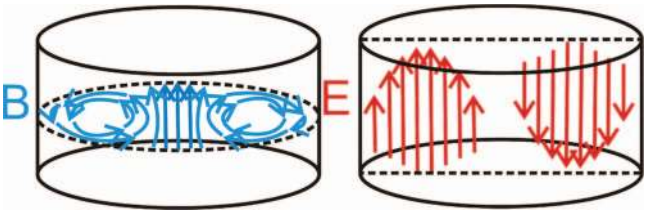

FIG. 3. A cross-sectional view demonstrating the electric and magnetic fields of the TM_{110} mode in a pillbox cavity.

however, zero at $r = 0$, and a transverse magnetic field that is maximal at $r = 0$, as seen in Figure 3. The TM_{110} mode is therefore ideally suited for transverse deflection of a beam, while minimally affecting the longitudinal beam properties. Transverse electric (TE) modes could be considered in the same manner, but due to the use of a dielectric which suppresses the electric field, these modes are not appropriately suited for a compact cavity.

The non-zero field components for the TM_{110} mode in cylindrical coordinates, where $r = \sqrt{x^2 + y^2}$ and θ are the radial and azimuthal coordinates, are compactly written, as (Lee[26])

$$E_z = \frac{2cB_0}{\sqrt{\varepsilon_r}}J_1(kr)\cos(\theta)\sin(\omega t), \tag{7a}$$

$$B_r = \frac{2cB_0}{r\omega\sqrt{\varepsilon_r}}J_1(kr)\sin(\theta)\cos(\omega t), \tag{7b}$$

$$B_\varphi = \frac{2B_0}{\sqrt{\varepsilon_r}}J_1'(kr)\cos(\theta)\cos(\omega t), \tag{7c}$$

where c is the speed of light in a vacuum, $k = \frac{\omega\sqrt{\varepsilon_r}}{c}$ is the wavenumber, ε_r is the relative permittivity of the dielectric material, and J_n is the nth order Bessel function. Here, the magnetic field amplitude B_0 is defined such that $B_y(r = 0) = B_0$, in agreement with Eq. (1) in Sec. II. The electric field E_z is also expressed in terms of B_0. The radius a of the cylindrical cavity is determined by the radial boundary condition for the electric field, $J_1(ka) = 0$; i.e., $ka = \frac{\omega a\sqrt{\varepsilon_r}}{c} \equiv p_{10} = 3.8317$, where p_{nm} is the mth zero of the nth order bessel function. For $f_0 = 3$ GHz, the radius of the TM_{110} mode vacuum pillbox cavity is $a = 6.1$ cm; the dielectric being considered ($\varepsilon_r = 37$) has a radius $a = 10$ mm. The length of the cavity, d, is determined by the maximum deflection possible for a traversing electron. For a passing electron to gain maximum deflection, it must enter when the magnetic field is at zero, and leave after half a period, or $d = \frac{v_e}{2f_0}$, where v_e is the velocity of the electron traversing the cavity longitudinally. In most electron microscopes electrons have energies in the range of 30–500 keV equating to velocities in the range of $\frac{c}{3} \le v_e \le c$. Combined with resonant frequencies of 3 GHz results in cavity lengths of $d = 1.7$–5 cm.

Following the treatment of a TE_{nml} dielectric filled pillbox by Pozar[27], the power loss P_{id} of an ideal lossless TM_{110} pillbox cavity is calculated to be

$$P_{id} = \frac{2\pi B_0^2 a}{\delta\mu_0^2\sigma}(d + a)J_0^2(p_{10}), \tag{8}$$

where μ_0 is the permeability of free space, σ is the conductivity of the metal, and $\delta = \sqrt{\frac{2}{\mu_0 \omega \sigma}}$ is the frequency dependent skin depth, resulting in $\delta = 1.2 \times 10^{-6}$ m for the case of copper at 3 GHz (Pozar[27]). The time averaged energy stored in the cavity can be calculated in a similar fashion,

$$U = \frac{\pi d B_0^2 c^2 \varepsilon_0 \varepsilon_r a^2}{4} J_0^2(p_{10}). \tag{9}$$

The quality factor $Q = \frac{\omega U}{P_{id}}$ of a pillbox cavity in the TM_{110} mode with imperfectly conducting walls but lossless dielectric is thus given by

$$Q = \frac{\omega \delta \mu_0 \sigma}{2} \frac{ad}{a+d}. \tag{10}$$

If a magnetic field amplitude of 3 mT is desired for a vacuum filled copper cavity operating at 3 GHz, with a radius of 6.1 cm and length of 1.7 cm, a stored energy of $U = 58$ μJ is found. For a copper cavity, the resulting power consumption is $P_{loss} = 98$ W, corresponding to a quality factor of $Q = 11\,100$.

To obtain high field strengths with lower power consumption, a vacuum filled cavity with a non-pillbox geometry was presented by van Oudheusden.[10] This cavity is operated in the same TM_{110} mode, requiring approximately 30 W of power. This is significantly lower than the vacuum pillbox, but is still a geometrically large cavity, with the radius being larger than the 6.1 cm radius of the vacuum pillbox. Further reduction in size and power consumption is wanted, both achievable with a proper dielectric filled cavity.

An ideal dielectric creates a reduction in the radius, a, of the cavity, thus decreasing the surface area of the metallic boundaries. Inspection of Eq. (8) shows it is clear that the power lost in an ideal dielectric will be less than in a vacuum filled counterpart, because the radius, a, decreases. If $\varepsilon_r \gg 1$, then $P_{id} \propto \frac{1}{\varepsilon_r}$. New advances in ceramic materials have allowed for the creation of dielectrics with $\varepsilon_r \geq 40$ at gigahertz frequencies (National Magnetics Group/TCI Ceramics[28]).

The ideal case only accounts for the power lost to the metallic walls of the miniature dielectric filled cavity. There is an additional power loss in the dielectric itself which must be accounted for. Assuming a frequency dependent complex permittivity, $\varepsilon_r = \varepsilon' + i\varepsilon''$, that induces a conduction current, the power loss in the dielectric is calculated:

$$P_d = \frac{\pi \omega B_0^2 c^2 d \varepsilon'' \varepsilon_0 a^2}{\varepsilon'} J_0^2(ka) + P_{id}. \tag{11}$$

Using Eqs. (8) and (11), the following equation is arrived upon for the power loss in a TM_{110} cavity filled with a lossy dielectric:

$$\frac{P_d}{P_{vac}} = \frac{1}{\sqrt{\varepsilon'}} \frac{\left(d/a_{vac} + 1/\sqrt{\varepsilon'}\right)}{\left(d/a_{vac} + 1\right)} + \frac{\varepsilon''}{\varepsilon'^2 \delta} \frac{d}{\left(d/a_{vac} + 1\right)}, \tag{12}$$

where P_{vac} is the power lost for a vacuum cavity with radius a_{vac} and the same magnetic amplitude B_0. Comparison between the stored energy U and the power loss in the dielectric P_d (Eqs. (9) and (11), respectively) shows that the Q for the lossy dielectric filled cavity follows (Pozar[27]):

$$Q_d^{-1} = Q_{id}^{-1} + \tan\delta, \tag{13}$$

where $\tan\delta = \frac{\varepsilon''}{\varepsilon'}$. Investigation of P_d as used in Eq. (12) combined with a material with a large ε_r and small $\tan\delta$, it is possible to design a pillbox cavity that is smaller in size and requires lower power to obtain the same desired field patterns and amplitudes along the z axis.

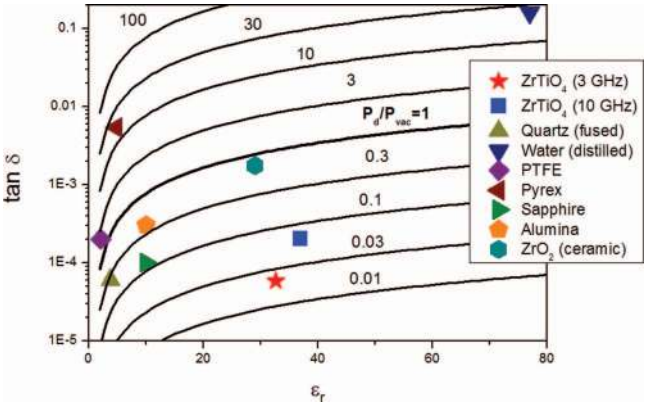

FIG. 4. A contour plot of P_d/P_{vac} as a function of $\tan\delta$ and ε_r. The lines represent values of constant P_d/P_{vac}. The symbols represent various common dielectric materials and their typical values measured at 3 GHz. The blue square represents the material chosen for filling the pillbox, while the red star represents our measured value.

Figure 4 is a contour plot of P_d/P_{vac} as a function of ε_r and $\tan\delta$. The curves indicate lines of constant P_d/P_{vac}. The symbols represent various materials that are well known, taken from Chao and Tigner[25]. The star and square represent the dielectric material chosen for this cavity, measured at 10 GHz by the company and at 3 GHz in our lab.

By carefully choosing an appropriate dielectric with a large relative permittivity and low loss tangent to fill the cavity, power loss can be reduced to less than a tenth of the power consumption a vacuum filled pillbox cavity requires for the same field amplitude and frequency.

C. Comparison of vacuum and dielectric filled pillbox

The dielectric chosen is a $ZrTiO_4$ ceramic doped with <20% $SnTiO_4$, seen in Figure 4. The relative permittivity was quoted by the company, T-Ceram, s.r.o.[29], as $\varepsilon_r = 36.5$–38 in the frequency range 0.8–18 GHz, with a loss tangent of $\tan\delta = 2 \times 10^{-4}$ only measured at 10 GHz. The desired operating frequency is 3 GHz, with a magnetic field amplitude of 3 mT, designed for 30 keV electrons. Table I shows the differences obtained in size and power consumption between the dielectric and vacuum cavities, with the given parameters aforementioned.

The table clearly shows that the dielectric cavity reduces drastically in radial size, as well as in the power loss. However, the addition of a dielectric material drops the quality factor quite dramatically as well. This effect manifests in the inverse relation between the loss tangent and the real part of the relative permittivity, as well as in the reduction in radial size

TABLE I. Comparison of estimated characteristics between vacuum and dielectric filled 3 GHz pillbox cavity with a magnetic field amplitude $B_0 = 3$ mT, relative permittivity $\varepsilon_r = 36.5$–38, and loss tangent tan $\delta = 2 \times 10^{-4}$.

	Vacuum pillbox	Dielectric pillbox
Radius (a)	60.98 mm	9.76 mm
Length (z)	17.1 mm	17.1 mm
Power loss	98.4 W	11.5 W
Quality Factor (Q)	11 100	2600

a, reducing Q_{id}. The total quality factor is calculated using Eq. (13).

III. PRACTICAL DESIGN

To accommodate practical restrictions upon the operation of the cavity, various adaptations were made to the ideal pillbox cavity to arrive at the final design that was implemented and tested in the beamline. These accommodations and their purposes are discussed in this section, followed by simulations to assure that the adaptations were not detrimental to the characteristics key to the operation of the cavity.

A. Physical adaptations

Beginning with a basic pillbox cavity of radius a length d, as seen in Figure 2, with the quoted $\varepsilon_r \approx 37.25$, $f_0 = 3$ GHz, and $v_e \approx \frac{c}{3}$, the dimensions of the dielectric inside the pillbox are found to be $d = 17.1$ mm and $a \approx 10$ mm. The surrounding metal shell is chosen to be copper, for its high conductivity, low cost, and ease of manufacturing.

For practical reasons, changes were added to the basic pillbox design. The adaptations to the cavity are divided into three main sections: electron pathway, side ports, and elliptical vacuum gaps. The first two are changes made to both the dielectric and the metal shell, while the third is purely to the metal shell.

The electron pathway is a 1 mm diameter hole running the length of the cavity along z. To avoid problems with charging, the diameter of the pathway through only the dielectric was enlarged to 3 mm, keeping the 1 mm diameter on the metallic shell, as can be seen in Figure 5.

Side ports located upon what will be defined as the x axis were added, extending through the metal shell and into the dielectric, seen in Figure 5. Upon one side, RF power is coupled into the cavity by means of a Hertzian dipole loop antenna (Orfanidis[30]), matching to the magnetic field through the loop. The antenna was designed for rotational freedom to allow for impedance matching for optimal power transfer to the fields.

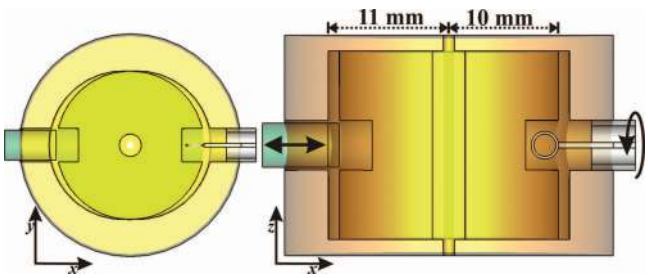

FIG. 5. Realistic dielectric filled cavity. The expanded radius in one direction further reduces frequency to the intended operating frequency.

The opposite side port was built to allow for the insertion of a tuning screw. An insertion of a dielectric plunger will decrease the resonant frequency f_0, while a metal plunger will increase the resonant frequency. This allows for a frequency tuning of ~20 MHz in either direction.

The relative permittivity of the dielectric was experimentally determined to be $\varepsilon_r \cong 32.7$ at 3 GHz, instead of 37 as expected. This gives a resonant frequency greater than can be corrected for by the tuning screw. To correct for the high resonant frequency, vacuum gaps were added to the metallic shell, lengthening the x-direction diameter to 22 mm, while keeping the y diameter at 20 mm, clearly visible in Figure 5. These vacuum gaps had a dual purpose. The first was to reduce the resonant frequency to the desired operating frequency. The second was to break the rotational symmetry of the pillbox. With rotational symmetry broken, the TM_{110} mode becomes two modes oriented in either x or y, with different resonant frequencies. The 2 mm difference in diameter between x and y results in 100 MHz peak-to-peak separation in the two TM_{110} modes, as will be discussed in part B below.

B. CST microwave studio simulations

The cavity is no longer an ideal pillbox, with deviations occurring off axis and breaking rotational symmetry. This realistic dielectric filled cavity is modeled in CST Microwave Studio[31] to determine deviations in the characteristics of the cavity from that of the ideal pillbox, particularly field profile characteristics along the beam trajectory at $r = 0$.

As previously mentioned, the relative permittivity was not as high as expected, leading to deviations from the initial pillbox cavity. To determine the proper ε_r, the frequencies of the two TM_{110} modes in simulations were matched with experiments (discussed in Sec. IV. RF cavity characterization), as seen in Figure 6.

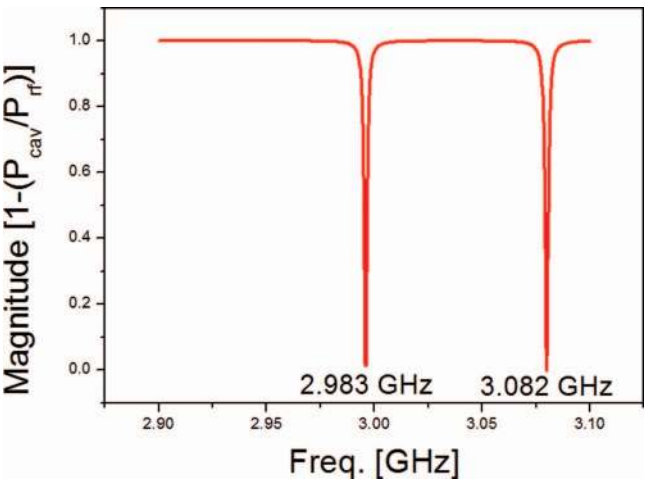

FIG. 6. Two TM_{110} modal frequencies after alterations to cavity.

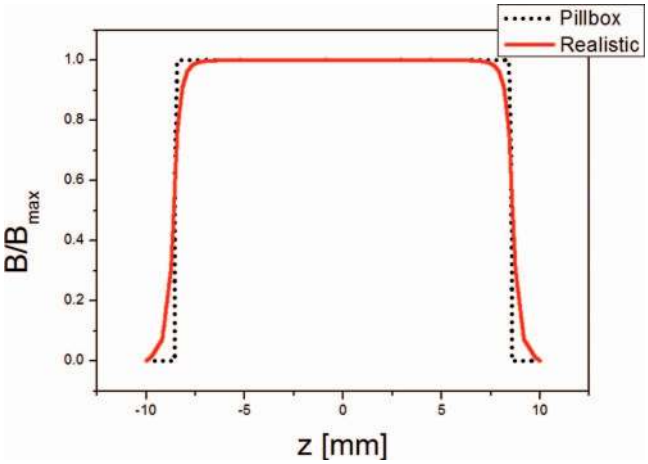

FIG. 7. The magnetic field profile along the longitudinal axis of the cavity at r = 0 for the realistic cavity geometry (red solid line) and the ideal pillbox cavity (black dotted line).

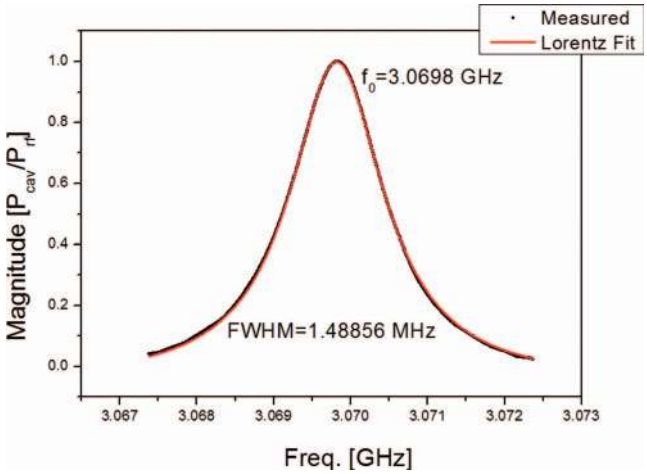

FIG. 8. The absorption spectrum of the cavity as a function of frequency with a Lorentzian fit.

To ensure that the field has not changed significantly along the interaction volume, the normalized magnetic field amplitudes B/B_{max} along the axis $r = 0$ are shown in Figure 7, both for an ideal pillbox cavity and the actual cavity geometry (Figures 2 and 5, respectively). As can be seen, the adjustments to the cavity have not significantly disturbed the ideal field configuration desired for the cavity.

To appropriately simulate losses and Q factor, the quoted loss tangent $\tan\delta = 2 \times 10^{-4}$ was also taken into account. As a result, the Q of the ideal pillbox was calculated to be 2600, while that of the simulated final cavity shifts to 2650; a negligible change in the Q of the cavity. With the correct permittivity, frequencies, Q factors and magnetic field profiles, it is reasonable to approximate the operation of the real cavity with that of the ideal pillbox.

IV. RF CAVITY CHARACTERIZATION

In this section, the cavity's operational characteristics are tested and checked before implementation into a beamline. The power absorption spectrum is measured, yielding the Q factor. Following is a field profile measurement along the longitudinal axis. Finally, a measurement of the frequency shift as a result of the tuning stub insertion depth is presented, demonstrating the frequency tunability of the cavity.

A. Power absorption

The ratio of the power absorbed by the cavity P_{cav} and the incident power P_{rf} as a function of frequency is described by a Lorentz curve with a full-width at half-maximum, $FWHM = \frac{2f_0}{Q_d}$ when matched. Figure 8 shows the absorption spectrum taken from a network analyzer, and fit with a Lorentz curve.

The total Q for the entire cavity is measured to be $Q_d = 4100$. This does not give agreement with the simulated $Q = 2650$, but suggests better. Using the calculated $Q_{id} = 5300$ and Eq. (13), the measured loss tangent is found to be $\tan\delta = 5.5 \times 10^{-5}$. This falls much lower than the quoted value $\tan\delta = 2 \times 10^{-4}$, making the power loss lower than expected. The large differences between the measurements and quoted values for the relative permittivity and loss tangent could be accounted for in the high frequency dependence of both the real and imaginary parts of the permittivity, as the company's quoted value was measured at 10 GHz, while the cavity is operated at 3 GHz. Simulations in CST using $\tan\delta = 5.5 \times 10^{-5}$ gives a total $Q_d = 4250$. This is much closer in agreement to the measured value.

B. Field profile

For measurement of the field profile along the electron trajectory, use of the so-called "bead pull" method is employed, based on the perturbation method of Maier and Slater,[32] manifesting as a shift in frequency based upon the cavity field strength at the location of the "bead."

Figure 9 compares the measured field profile to the field profile calculated with CST Microwave Studio for the TM_{110} mode. The general shape is in agreement with what would be expected for the TM_{110} mode. The discrepancies appearing

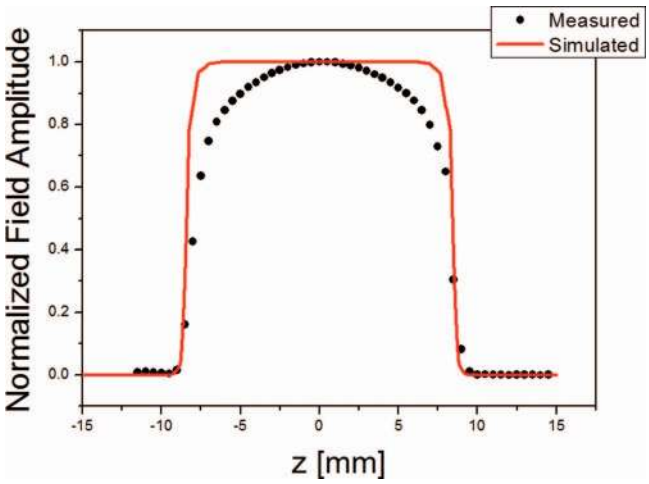

FIG. 9. Field profile measurement (black circles) and calculated field profile (red solid curve) of the TM_{110} mode.

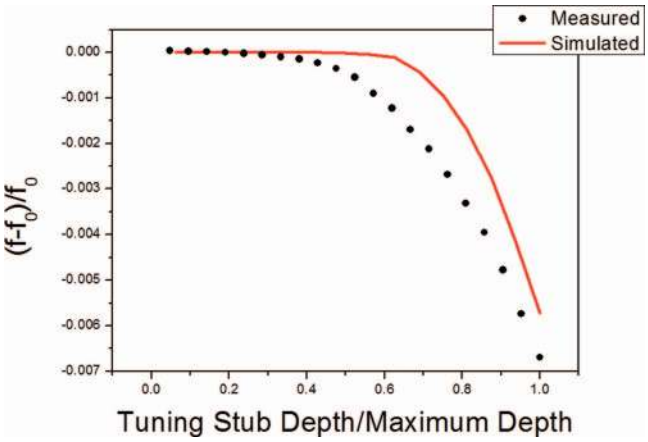

FIG. 10. Frequency shift versus the depth of the dielectric tuning stub, measurement (black dots) plotted against CST Microwave Studio simulation (red solid curve).

when the metal bead is close to the copper shell enfixing the dielectric material, can be attributed to mirror charges (Kiewiet[33]) and fringe fields which are present at the entrance and exit holes.

C. Tuning screw

A dielectric tuning stub was made from the same dielectric material as the inner portion of the cavity. The tuning stub is inserted into the side of the cavity, entering through the vacuum area, and into the dielectric filling inside of the cavity. Since more dielectric is added to the effective volume of the cavity, the frequency decreases. Figure 10 shows this behavior; as the dielectric tuning stub is inserted into the port, the frequency shifts down.

The tuning range with the dielectric tuner is a maximum of 21 MHz, in reasonable agreement with CST Microwave Studio simulations. The difference between simulations and measurements may point to anisotropy in the relative permittivity (Chen *et al.*[34]) or the dielectric filling shifting inside the cavity.

V. OPERATIONAL USE

In this section, the implementation in an altered electron microscope beamline is discussed. Streaking of the electron beam is demonstrated, and the length of the streak is measured at various input powers. Following preliminary measurements of the normalized transverse emittance of the chopped beam is compared to numerical particle tracking simulations.

A. Streaking and chopping

The cavity was mounted in the beamline of a 30 keV tungsten hairpin SEM (Philips XL-30). Power was then fed to the cavity with a tunable 16 W peak continuous wave amplifier, allowing for a maximum magnetic field amplitude of $B_0 = 4.3$ mT. The schematics as implemented are seen in Figure 11.

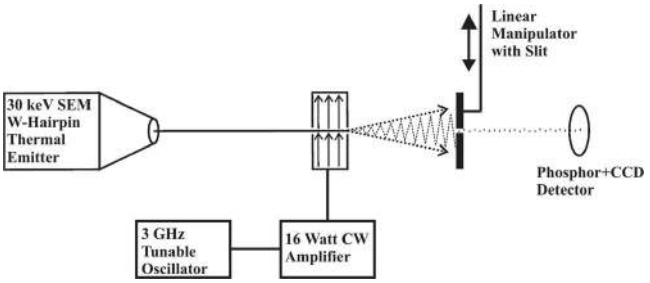

FIG. 11. General schematics demonstrating the beamline that the cavity was designed for and tested in.

Figure 12(a) is a beam on a phosphor screen from a 30 keV SEM at a distance $L = 20.5$ cm from the cavity with no power fed in. Figure 12(b) is an image of the phosphor screen with $P_{rf} = 3.2$ W RF power fed into the cavity, giving rise to a streak length of $\chi = 15$ mm, corresponding to a magnetic field amplitude $B_0 = 2$ mT.

According to theory, the magnetic field amplitude required for a streak length χ is given by

$$B_0 = \frac{m\omega}{4Lq}\chi, \tag{14}$$

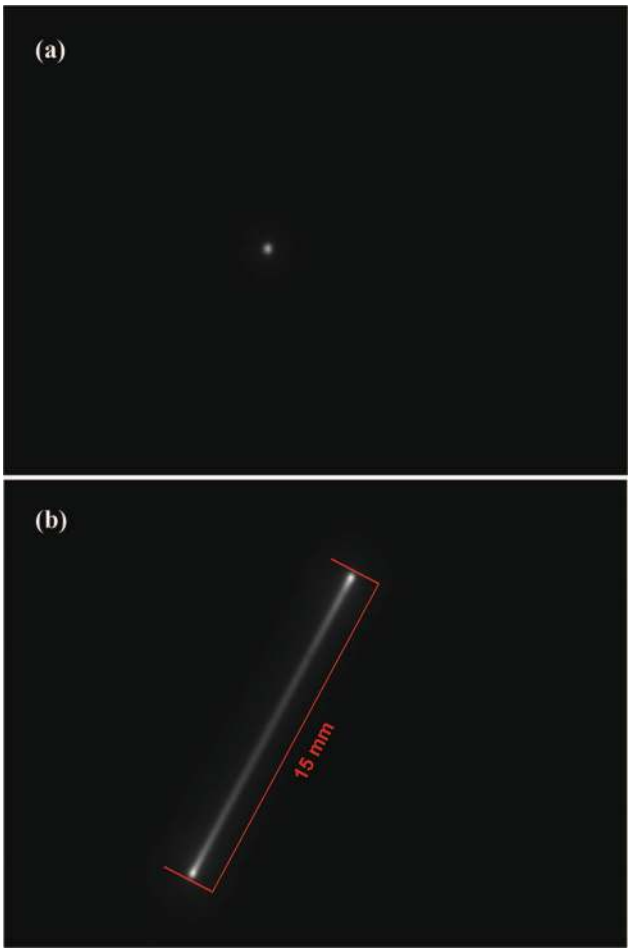

FIG. 12. (a) Electron spot on detector with no power fed to the cavity. (b) Streak electron beam on detector with $P_{rf} = 3.2$ W power fed to the cavity.

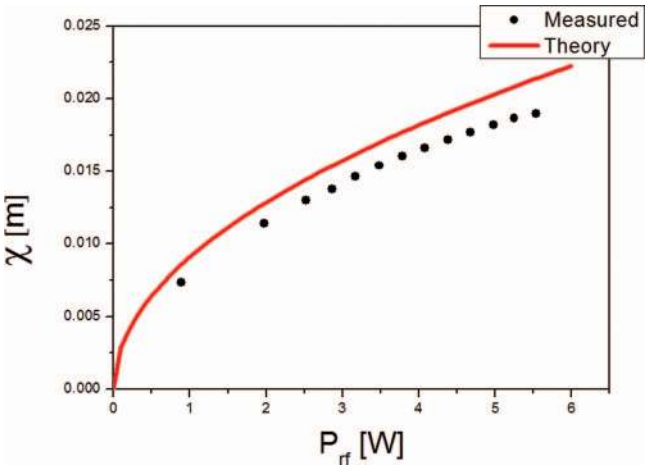

FIG. 13. Theoretical (red solid line) and measured (black dots) streak length of the electron beam at the detector as a function of RF input power.

where the relation $\chi = 2L\alpha(\varphi_0 = \pi/2)$ was used, with $\alpha(\varphi_0)$ taken from Eq. (4); $\varphi_0 = \pi/2$ corresponds to a maximum deflection for the incoming electrons. Plugging Eq. (14) into Eq. (11), along with $\varepsilon_r = 32.7$ and $\tan\delta = 5.5 \times 10^{-5}$, the theoretically required RF power P_{rf} is found, which is plotted in Figure 13.

Streak length χ was measured for various settings of RF input power P, as shown in Figure 13. Calculating back from the highest measurement point on Figure 13, it is found that with an input power of 5.5 W, a field amplitude of 2.54 mT is obtained in the cavity. A slit size of 10 μm at a distance of 10 cm after the cavity would result in 110 fs pulses. Satisfactory agreement between theory and measurements is obtained: the system performs as expected. At higher power input, the cavity was operated at a higher temperature, which possibly explains the small discrepancy between the measurements and the theoretical predictions. Konaka *et al.*[35] observed an increase in loss tangent at higher temperatures for many ceramic materials, including ZrO_2, which could account for the difference.

B. Normalized transverse emittance

A figure of merit for the quality of a beam is the current density per unit solid angle, or brightness, defined as $B = \frac{I}{\Delta A \Delta\Omega}$, where I is the current, ΔA is the spread in the transverse area, and $\Delta\Omega$ is the spread in the solid angle. To compare beams of different energies, the reduced brightness should be used. It can be shown that the reduced brightness can be written as $B_r = \frac{2q}{mc^2}\frac{I}{4\pi\varepsilon_{N,x}\varepsilon_{N,y}}$, where the normalized emittance in the x-direction is defined as $\varepsilon_{N,x} \equiv \frac{1}{mc}\sqrt{\langle x^2\rangle\langle p_x^2\rangle - \langle x p_x\rangle^2}$ with p_x being the x-momentum and brackets denoting averaging over the entire beam (Luiten *et al.*[36]). The y-emittance is defined analogously.

Here, it is clear that for high brightness beams at a given current, a small emittance must be obtained. The emittance is a measure for the focusability of a beam; for a given focusing angle, the smaller the emittance, the smaller the spot size at the focus. Because the act of chopping the beam reduces the current by ~3 orders of magnitude, to compare the chopped beam with the dc beam entering the cavity, the emittances of the two should be employed, rather than the brightness. This is done using the quadrupole waist scan method.

Extending the beamline, and adding a quadrupole focusing magnet between the slit and detector, a waist scan was performed upon the electron beam, varying the focal distance of the magnet and measuring the spot size on the detector. To first order approximation, the beam will have a RMS size σ_x on the detector given by

$$\sigma_x = \sqrt{[l_1 l_2 - (l_1+l_2) f_{quad}]^2 \frac{\varepsilon_{N,x}^2}{\gamma^2\beta^2\sigma_v^2 f_{quad}^2} + (f_{quad} - l_2)^2 \frac{\sigma_v^2}{f_{quad}^2}}, \quad (15)$$

where l_1 is the distance from the (virtual) source to the quadrupole magnet, l_2 is the distance from the quadrupole magnet to the detector, f_{quad} is the focal length of the quadrupole, σ_v is the virtual source RMS size, $\beta = v/c$ is the normalized velocity, and $\gamma = (1-\beta)^{-1/2}$ is the relativistic Lorentz factor (van Oudheusden[37]). The equation assumes the magnet to act like a thin lens, and that the beam behaves as if it had originated from a virtual source of size σ_v located at a distance l_1 before the magnet. The values l_1 and l_2 are known, so plotting σ_x as a function of f_{quad}, and fitting σ_v yields a value for the normalized transverse emittance. These measurements were applied to the normal dc beam, and again to the chopped beam, as seen in Figure 14.

The waist scan of the dc beam yielded a transverse emittance of $\varepsilon_{n,x}^{dc} = 9 \times 10^{-10}$ mrad, a very standard value for an older tungsten hairpin emitter system. The corresponding emittance with the cavity turned on and the slit moved into place was $\varepsilon_{n,x}^{strk} = 9 \times 10^{-9}$ mrad. This is an increase by an order of magnitude but still yields a beam quality comparable to or perhaps better than photo-cathode driven systems.

For comparison, the beamline was simulated in GENERAL PARTICLE TRACER (GPT),[38] a numerical particle tracking program. The electron beam entering the cavity was modeled in GPT using the measured normalized transverse emittance of the dc beam $\varepsilon_{n,x}^{dc} = 9 \times 10^{-10}$ mrad, traversing the cavity with the same beam characteristics (size and angle) as the measurement. The cavity was modeled using the realistic fields from CST Microwave Studio, imported into GPT, oscillating at 3 GHz with an on axis magnetic field amplitude of 2 mT, followed by a slit of 50 μm a distance of 8.5 cm measured from the center of the cavity. After the slit, GPT predicts the electrons have an emittance of 7.5×10^{-9} mrad, approximately in agreement with the measured value of 9×10^{-9} mrad, demonstrating that the cavity can be operated with a comparable peak brightness to that of many photocathode driven systems.

The particle tracking code can be used to investigate the cause of the emittance growth. Inspection of the simulated phase-space distribution of the chopped beam revealed that the transverse phase-space distribution is highly correlated with the longitudinal (or temporal) position of the electrons (this could also be stated as the entrance phase of the cavity fields for a given electron). This implies that a method for minimizing the transverse emittance growth as a result of the cavity can be developed.

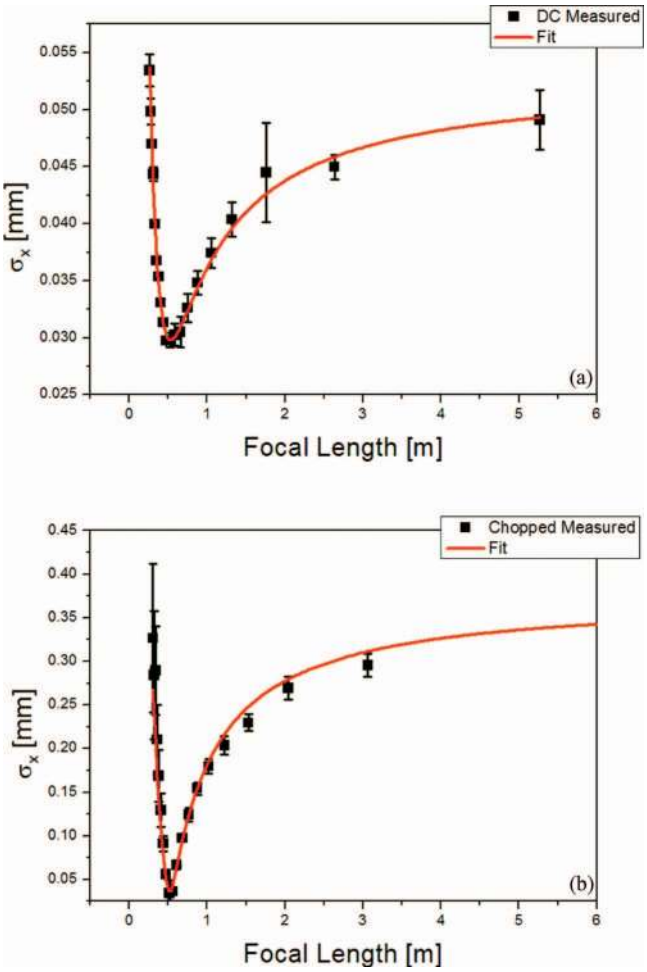

FIG. 14. Waist scan measurements of (a) the dc beam and (b) the chopped beam. The red curves are fits using Eq. (15). The fits yield normalized transverse emittances of 0.9 and 9 nm rad for the dc and the chopped beams, respectively.

Further simulations have suggested that a number of factors play a role in the emittance growth. These factors include, but are not limited to, the initial size and angle of the beam at the cavity entrance, the initial emittance of the beam, and phase of the cavity field. Because of so many parameters being influential to the beam quality, further optimization seems likely. The narrower the beam, the less emittance growth; this leads to the conclusion that better beams lead to less emittance growth. A comprehensive study of the beam dynamics as a result of the cavity will be presented in a following publication.

VI. CONCLUSION

A high permittivity/low loss dielectric was used to design and build a TM_{110} cavity for the purpose of creating sub-picosecond electron bunches delivered at a high repetition rate. It was demonstrated that the cavity is smaller and more power efficient than the vacuum filled equivalent. The cavity was built with a large frequency tuning capability. The cavity was mounted in a 30 keV SEM beamline and demonstrated operational by streaking the electron beam in one direction, allowing for the creation of a regular train of sub-picosecond electron pulses. The transverse emittance of the pulses was measured, demonstrating that a high peak brightness within the pulses can be maintained. Because the cavity is compact, power efficient, simple, and easily synchronized with femtosecond lasers, all with minimal beam degradation, it provides an alternative time-resolved tool for the electron microscopy community.

In addition to being used for time-resolved measurements, the creation of ultra-short electron bunches also opens the possibility of time-dependent aberration correction. The use of time-dependent lenses and their fields to circumvent Scherzer's theorem has long been known; but has been considered too difficult based on the transit time and phase dependency (Schoenhense and Spiecker[39]). Well characterized short pulses could be used, in combination with time-dependent lenses, to compensate the spherical and chromatic aberration that occurs in static field lens systems.

ACKNOWLEDGMENTS

The authors would like to thank the technical support of E. Rietman, L. van Moll, H. van Doorn, and I. Koole whose knowledge and expertise made the project operational. Also, the internship work of E. Vos and J. Daniels gave great insight towards the project. Thanks are also greatly offered to FEI for financial and technical support for the project and the donation of a 30 keV SEM to build a beamline. This work is part of the research program of the Foundation for Fundamental Research on Matter (FOM), which is part of the Netherlands Organization for Scientific Research (NWO).

[1] G. S. Plows and W. C. Nixon, J. Phys. E: Sci. Instrum. **1**, 595 (1968).
[2] L. C. Oldfield, J. Phys. E: Sci. Instrum. **9**, 455 (1976).
[3] A. Gopinath and M. S. Hill, J. Phys. E: Sci. Instrum. **10**, 229 (1977).
[4] E. Hieke and G. Meusburger, Rev. Sci. Instrum. **49**, 802 (1978).
[5] H. Sadorf and H. A. Kratz, Rev. Sci. Instrum. **56**, 567 (1985).
[6] K. Ura, H. Fujioka, and T. Hosokawa, Rev. Sci. Instrum. **49**, 1293 (1978).
[7] L. C. Oldfield, Ph.D. dissertation, University of Cambridge, Cambridge, 1973.
[8] P. W. Hawkes and E. Kasper, *Principles of Electron Optics* (Academic, New York, 1989), pp. 872–876.
[9] A. Gahlmann, S. T. Park, and A. H. Zewail, Phys. Chem. Chem. Phys. **10**, 2894 (2008).
[10] D. Shorokhov and A. H. Zewail, Phys. Chem. Chem. Phys. **10**, 2879 (2008).
[11] A. H. Zewail, Science **328**, 187 (2010).
[12] F. Carbone, B. Barwick, O. H. Kwon, H. S. Park, J. S. Baskin, and A. H. Zewail, Chem. Phys. Lett. **468**, 107 (2007).
[13] J. Yang, F. Sakai, T. Yanagida, M. Yoruzu, Y. Okada, K. Takasago, A. Endo, A. Yada, and M. Washio, J. Appl. Phys. **92**, 1608 (2002).
[14] T. van Oudheusden, J. R. Nohlmans, W. S. C. Roelofs, W. P. E. M. Op't Root, and O. J. Luiten, Ultrafast Phenom. XVI **92**, 938 (2009).
[15] J. Cao, Z. Hao, H. Park, C. Tao, D. Kau, and L. Blaszczyk, Appl. Phys. Lett. **83**, 1044 (2003).
[16] M. R. Armstrong, K. Boyden, N. D. Browning, G. H. Campbell, J. D. Colvin, W. J. DeHope, A. M. Frank, D. J. Gibson, F. Hartemann, J. S. Kim, W. E. King, T. B. LaGrange, B. J. Pyke, B. W. Reed, R. M. Shuttlesworth, B. C. Stuart, and B. R. Torralva, Ultramicroscopy **107**, 356 (2007).
[17] H. S. Park, J. S. Baskin, B. Barwick, O. H. Kwon, and A. H. Zewail, Ultramicroscopy **10**, 7 (2009).
[18] A. Yurtsever and A. H. Zewail, Science **326**, 708 (2009).
[19] P. Baum and A. H. Zewail, Chem. Phys. Lett. **462**, 14 (2008).
[20] A. Kubo, K. Onda, H. Petek, Z. Sun, Y. S. Jung, and H. K. Kim, Nano Lett. **5**, 1123 (2005).

[21]F. B. Kiewiet, A. H. Kemper, O. J. Luiten, G. J. H. Brussaard, and M. J. van der Wiel, Nucl. Instrum. Methods Phys. Res. A **484**, 619 (2002).
[22]T. M. Fortier, A. Bartels, and S. A. Diddams, Opt. Lett. **31**, 1011 (2006).
[23]A. Bartels, T. Dekorsy, and H. Kurz, Opt. Lett. **24**, 996 (1999).
[24]A. Bartels, D. Heinecke, and S. A. Diddams, Opt. Lett. **33**, 1905 (2008).
[25]A. W. Chao and M. Tigner, *Handbook of Accelerator Physics and Engineering* (World Scientific, Singapore, 1999), pp. 359–360, 369–380.
[26]S. Y. Lee, *Accelerator Physics*, 2nd ed. (World Scientific, Singapore, 2004), pp. 343–355.
[27]D. M. Pozar, *Microwave Engineering*, 3rd ed. (Wiley, Hoboken, 2005).
[28]See http://www.magneticsgroup.com/tci.htm for company information.
[29]See http://www.t-ceram.com/dielectric-resonators.htm for company information.
[30]S. J. Orfanidis, *Electromagnetic Waves and Antennas* (Rutgers University, Camden, 2010), p. 652.
[31]See http://www.cst.com for Computer Simulation Technology, CST Microwave Studio 2011.
[32]L. C. Maier, Jr. and J. C. Slater, J. Appl. Phys. **23**, 68 (1952).
[33]F. Kiewiet, Ph.D. dissertation, Eindhoven University of Technology, Eindhoven, The Netherlands, 2003.
[34]L. F. Chen, C. K. Ong, C. P. Neo, V. V. Varadan, and V. K. Varadan, *Microwave Electronics:Measurement and Materials Characterization* (Wiley, West Sussex, 2004), p. 323.
[35]T. Konaka, M. Sato, H. Asano, and S. Kubo, J. Supercond. **4**, 283 (1991).
[36]O. J. Luiten, B. J. Claessens, S. B. van der Geer, M. P. Reijnders, G. Taban, and E. J. D. Vredenbregt, Int. J. Mod. Phys. A **22**, 3882 (2007).
[37]T. van Oudheusden, Ph.D. dissertation, Eindhoven University of Technology, Eindhoven, The Netherlands, 2010.
[38]See http://www.pulsar.nl for Pulsar Physics, General Particle Tracer (GPT) code.
[39]G. Schoenhense and H. Spiecker, J. Vac. Sci. Technol. B **20**, 2526 (2002).